of the XRD results, similar to that observed by Okubo et al.[69], along with magnetic susceptibility data that indicates the presence of unpaired electrons. X-ray diffraction (XRD) data indicates the formation of pure single-phase $LiCoO_2$ for the 20, 30 and 40 nm samples, all the peaks corresponding to the layered α-$NaFeO_2$ structure (Figure 4.3a). Lattice parameters are extracted and the c/a ratio is approximately 4.99, indicating a well-formed layered structure.[81] Detailed information regarding the lattice parameters is given in Table 4.2. The reflections in the XRD pattern for the 10nm particles are broad and a quantitative refinement could not be achieved.

X-ray photoelectron spectroscopy (XPS) was carried out with a Thermo-Scientific K-Alpha spectrometer using a focused monochromatic Al Kα anode source. As shown in Figure 4.3b, all compounds show a Co $2p_{3/2}$ main peak at 779.5eV with a satellite peak at 789.5eV and a Co $2p_{1/2}$ main peak at 794.5eV with a satellite peak at 804.5eV. This observation confirms that the oxidation state is Co^{3+}. This is strong evidence that our nano-sized LiCoO2 samples are stoichiometric. Co^{2+} coordinated by oxygen is characterized by a strong broadening of the main line and a very intense satellite peak at 785.5 eV (Co $2p_{3/2}$) and 802.5 eV (Co $2p_{1/2}$),[80,82] which are both absent in the spectra.

^{7}Li magic-angle-spinning (MAS) NMR spectroscopy was performed at a magnetic field strength of 4.7 T with a spinning speed of 35 kHz to explore the Li nonstoichiometry in nano-sized $LiCoO_2$. Figure 4.4a shows that the spectra of the 10 to 30 nm particles are dominated by a single resonance at 0 ppm, as expected for a stoichiometric, diamagnetic $LiCoO_2$ sample.[72] The larger NMR linewidth observed for the 10 nm sample compared to the others may be due to the presence of a trace amount (<1%) of Co_3O_4 impurity, which results in faster transverse relaxation leading to larger line width. A weak, hyperfine shifted resonance is observed at +185 ppm for the 30 nm sample. This shift, along with peaks at 3, -6 -16, -40 ppm (not observed in our system here, presumably because they are too weak) were previously suggested to be associated with excess Li ions that replace Co^{3+} sites in the bulk, resulting in a defect structure discussed above, with two adjacent square-based pyramids containing two intermediate-spin Co^{3+} ions per oxygen vacancy.[72] Even in the 30 nm sample, the percentage of excess Li is only approximately 0.6%. Two new hyperfine-shifted resonances were observed at -115 and -260 ppm (Fig. 4.4b), which are attributed to the presence of intermediate and/or high spin Co^{3+} (IS, HS). To the best of our knowledge, these shifts have not been reported in the literature. An analysis of the spin density on the {104} surface, as shown in Figure 4.2(b), indicates that the Li^+ ions on this surface contain negative spin density and will thus give rise to a negative shift. Integration of the spin density around the Li nucleus to 0.8 Å, using the approach developed by Carlier et al.[83] confirms this observation and indicates that the Li nuclei in the subsequent {104} surface is negative, while the spin density of the Li in the layer below is smaller, but positive (and thus it may be difficult to resolve from the intense bulk $LiCoO_2$ resonance/and or be buried under the spinning sidebands). Further calculations will focus on the direct calculations of hyperfine shifts[84,85] on this and a wider range of surfaces. Importantly, quantitative fitting of the NMR spectra to extract the concentration of Li^+ ions nearby paramagnetic Co ions, confirms that the percentage of paramagnetic ions increases with decreasing particle size.

Magnetic measurements were performed, using a superconducting quantum interference device (SQUID), at a magnetic field of 1.0 T in the temperature range of 5-

300K. The molar magnetic susceptibility of the various sized nano-$LiCoO_2$ particles are plotted as a function of temperature in Figure 4.5a. The magnetic susceptibility of bulk $LiCoO_2$ is low and practically temperature independent, which is attributed to a Van Vleck-type of paramagnetism associated with diamagnetic Co^{3+} (LS) in the layered structure.[86] In contrast, our nano-size $LiCoO_2$ exhibits a typical Curie-Weiss behavior for $T>100K$. The Curie constant was determined in the temperature range of 200-300K. The Curie constant increases with decreasing particle size and fitting of the Curie constant indicates that the molar Curie constant is as high as 0.20 in 10nm-sized $LiCoO_2$.

Careful transmission electron microscopy (TEM) examination of the nano-sized $LiCoO_2$ shows that all particles exhibit plate-like morphology, plates corresponding to the {001} planes; the edges are dominated by the {104} planes justifying our computational study of this surface. If the planes are terminated by the {001} surface, according to first principles computation of this work and previous work by Kramer and Ceder,[79] Co^{3+} remains octahedrally coordinated with a low-spin configuration. The contribution of Co^{3+} (IS) on the {104} and the Co^{3+} (HS) on the {110} surfaces are most likely attributing to the abnormally high magnetic susceptibility seen in nano-size $LiCoO_2$.

The proposed electronic spin state of the surfaces relevant for (de)intercalation has significant impact on the lithium (de)intercalation voltage profile, as revealed by first principles computation performed to calculate the Li extraction potential from different surfaces. If Co^{3+} remains as LS on the {104} surface, the voltage of lithium extraction is as low as 2.32V; by contrast, when a spin transition from LS to IS occurs, the voltage of lithium extraction is 3.69V, close to the bulk value of 3.65V. The narrowing energy gap between the occupied and unoccupied states in IS and HS state Co ions indicates that the insulating nature of $LiCoO_2$ can be altered due to the change in spin state (see Figure 4.6). This helps in explaining the fact that in the lithium half-cell with nano-sized $LiCoO_2$ as the cathode, a clear first order phase transition, associated with the metal-insulator-transition, is absent as no flat voltage plateau is observed upon the first charge[87] (see Figure 4.7).

4.1.4 Conclusions

In conclusion, it is proposed in this work that electronic spin state transitions occur on the surfaces of stoichiometric $LiCoO_2$, where trivalent cobalt ions adjacent to the surface adopt an intermediate spin state if it they are square pyramid coordinated and a high spin state if they are pseudo-tetrahedrally coordinated. This phenomenon is quantified in nano-sized stoichiometric $LiCoO_2$. We also observed in first principles calculations that both {104} and {110} surfaces with optimized electronic spin states expand normal to the surface and the displacement is of the order of 0.1-0.2Å. This work suggests that changes in electronic spin state could be a common phenomenon in transition metal oxides. The low coordinated geometries on the surface of the oxides result in spin states that are distinct from the bulk. Consequently, unique magnetic and electronic properties arise and alter the materials performance in devices. We show that in this case, the voltage profile of (de)intercalation is dramatically changed. It is therefore promising to control the surfaces and interfaces of nano-sized materials to alter the electronic and magnetic properties, significantly different from the bulk behaviors.

4.2 The Role of $LiCoO_2$ Surface Terminations in Oxygen Reduction and Evolution Kinetics

4.2.1 Introduction

Recent studies have shown that electronic structure features of oxides such as e_g occupancy[88-90] of transition metal ions could govern the ORR/OER activities of transition metal oxides, where having an e_g occupancy close to unity showed maximum specific ORR and OER activity.[88,89] More recently, it has been found that moving the O p band center closer to the Fermi level leads to much enhanced specific OER activity.[91] In addition, a better flexibility of transition metal atoms to adopt various oxidation and spin configurations is also correlated to higher OER activity.[92]

From the previous studies, it has been reported the nanosized stoichiometric rod-shaped $LiCoO_2$ rods have low-spin Co^{3+} on the nanorod sides terminated with (003) facets and intermediate- or high-spin Co^{3+} on tips that are usually dominated by high-index surfaces such as (104).[93] The difference would result in the electronic structure differences from tips to sides, with a narrowing in band gap for the spin-transited Co^{3+} on the tips compared to the sides from the DOS (density of states) calculations. The corresponding electrochemical performance alters from the nanorods to the bulk $LiCoO_2$, lacking a plateau corresponding to the metal-insulator transition.

In this study, the ORR and OER activities and pseudo-capacitance of these rod-shaped $LiCoO_2$ were studied in 0.1 M KOH. Higher specific ORR and OER activities accompanied by higher charge transfer per surface area during Co 2+/3+ and 3+/4+ redox processes were found at the tips, compared with the side surfaces (due to the difference in e_g occupancies for sides and tips)

4.2.2 Methodologies

4.2.2.1 Electrochemical Measurements

The rotating disk electrode (RDE) configuration was employed for electrochemical measurements. All potentials were calibrated to the reversible hydrogen electrode (RHE) using H_2/H^+ redox. $LiCoO_2$ samples were mixed with the oxides: AB carbon: Nafion® ratio of 5:1:1, and the oxides loading on the disk is 0.25 mg/cm^2_{disk}. All electrochemical measurements were done in 0.1 M KOH, with IR (resistance determined using electrochemical impedance spectroscopy) and double-layer capacitance corrections when available. All measurements were repeated 3 times to establish good reproducibility.

4.2.2.2 Transmission Electron Microscopy

TEM images were taken on JEOL 2010F with a point resolution of 0.19 nm, used to determine particle size distributions and general morphology of the catalyst nanoparticles. High resolution TEM images were formed without an objective aperture and were analyzed using Gatan Digital Micrograph v2.01 (Gatan Inc.). $LiCoO_2$ particles were assumed to have a rod shape with different sizes and are noted using their average diameters of 9nm, 14nm, 31nm and 40 nm, determined by TEM images. The surface areas were computed using the particle dimension distributions (Figure 4.8c) collected from TEM images and the following equations[94]:

$$S_{tip} = \frac{\sum_i 2\pi D_i^2/4}{\rho \sum_i \pi D_i^2 L_i/4} = \frac{2\sum_i D_i^2}{\rho \sum_i D_i^2 L_i} \qquad \text{Eq. 1}$$

$$S_{side} = \frac{\sum_i \pi D_i L_i}{\rho \sum_i \pi D_i^2 L_i/4} = \frac{4\sum_i D_i L_i}{\rho \sum_i D_i^2 L_i} \qquad \text{Eq. 2}$$

$$S_{total} = S_{tip} + S_{side} \qquad \text{Eq. 3}$$

where ρ is the density of bulk $LiCoO_2$, D_i and L_i are the diameter and length of $LiCoO_2$ nanoparticles.

4.2.2.3 EELS

Electron Microscopy work was carried out on a Cs-corrected FEI Titan 80/300-kV TEM/STEM microscope equipped with a Gatan Image Filter Quantum-865. All EELS spectra were acquired at 60 kV and with a beam size of ~0.7Å, except for those of control measurements samples which were acquired at 300 kV. Judged from the full width at half height (FWHH) of the zero loss peak, the energy resolution is ~1eV. EELS spectra shown in this work were acquired from a rectangular area of ~1 X 2 nm with an acquisition time of 3 seconds and a collection angle of 39mrad. For each sample, at least six particles' (six side-tip sets) spectra were collected. The energy axis was calibrated using the zero loss peak.

4.2.3 Results and Discussions

The $LiCoO_2$ nanorods were characterized firstly by transmission electron microscopy (TEM). These nanorods have similar morphologies but different sizes and were denoted by their average diameter of 9, 14, 31 and 40 nm (Figure 4.8). The calculation of tip and side surface areas can be found in Table 4.4. The geometric ORR and OER activity in Figures 4.11 suggested that the smaller the particle size, the higher the total activity, due to the higher total surface area of the smaller nanorods. The tip surfaces are ~10 times more active for ORR than the side surfaces, and the difference is ~4 times in OER. In addition to OER and ORR, the tip of $LiCoO_2$ nanorods was found to be more redox active than the side surfaces in the redox of surface Co atoms, shown in Figure 4.12.

Electron energy loss spectroscopy (EELS) analysis of $LiCoO_2$ nanorods suggested that the tips could have lower hybridization of Co-O bounds than the sides. Representative EELS spectra of the pristine 9-nm sample are shown in Figure 4.9a and b, where the position of EELS acquisition is shown in Figure 4.10. The Co L_3/L_2 ratios of ~2.7 were comparable to those of our previous XPS results,[93] indicative of Co oxidation state of 3+, and no noticeable changes in the Co L_3/L_2 ratio was observed between side and tip. For O K spectra, the area of the pre-peak was linearly proportional to the product of the total number of the empty O 2p − Co 3d states (4 for Co^{3+} considering equal weighting of e_g and t_{2g} electrons) and their extent of hybridization.[90] The quantitative analysis of the difference of O pre-peak areas between sides and tips can be found in Table 4.5, where the side of pristine $LiCoO_2$ showed a ~20% larger pre-peak area in the O K-edge than the tip at around 532 eV, consistent with our previous study on $LiCoO_2$ nanorods.[93] The smaller pre-peak on tips suggested an intermediate- or high-spin Co^{3+} with weaker hybridization of O 2p and Co 3d, originated from the under-coordinated Co atoms on tip surfaces, [93] while the fully-coordinated Co atoms on nanorod sides have a low-spin state with a greater degree of O 2p and Co 3d hybridization. Such difference in electronic structures between tips and sides could play an important role in surface catalytic reactions.

The surface Co redox can also be confirmed from EELS: after ORR the Co L3/L2 ratio increased from original ~2.7 to ~3.8 for tips and to ~3.1 for sides (Figure 4.9c and Table 4.7), indicating the partially reduction of surface Co atoms[95]; while after OER, the

L3/L2 ratio decreased to ~2.5 for tips and is still ~2.7 for sides (Figure 4.12a and Table 4.7), indicating the partially oxidation of Co on tips. The change of L3/L2 ratios on tips are larger than on sides, and the change after ORR is larger than after OER, which is also in consistent with the result that tips have larger charge transfer than side and Co2+/3+ redox process has larger charge transfer than 3+/4+ redox.

After ORR or OER measurements (holding at 0.7 or 1.55 V vs. RHE for 1 h), 50% of $LiCoO_2$ nanorods examined were found to have maintained a smaller O K pre-peak on the tip (peak area <3.5, similar to the pristine tip) than that on the side (peak area >4, similar to the pristine side), as shown in Figures 4.9d, 4.12b and case 1 in Table 4.5. This indicates the open structure can be at least partially kept during OER and ORR on the tip. This can explain the higher ORR/OER activities of the tip as compared to the side, since the open structure and the under-coordinated Co ions on tips can adsorb oxygen species from the electrolyte more easily and therefore could promote ORR kinetics at the side, with the oxygen being more easily to dissociate/intercalate.[88,89,92] We also found 50% of the $LiCoO_2$ nanorods showed comparable O K pre-peak areas between tip and side after OER or ORR, all close to the pre-peak of pristine side surface (peak area ~4.5), as shown in Figures 4.9f, 4.12d and case 2 in Table 4.5. This can also be observed in a control experiment with the pristine sample immersed in O_2-saturated 0.1 M KOH electrolyte for 1 h (Figure 4.14 and Table 4.5). This changing of tip pre-peak area is probably due to the under-coordinated surface Co on the tip getting bonded by water or OH/OOH groups and then the surface reconstructed, making the coordination and chemical environment of Co atoms on the tip become similar to that on the side. During control experiment, the $LiCoO_2$ nanorods statically contacted and adsorbed water or OH/OOH groups for a long time, which led to the gradually reconstruction of all the under-coordinate Co on tips; while during ORR or OER, the OH/OOH group adsorbed on under-coordinate Co ions is continuously consumed and re-adsorbed, and therefore the active Co sites on the tip surface are cyclically regenerated without long-time OH/OOH group adsorption, which might be the reason that only some of the nanorods lost their under-coordinated tips after ORR or OER.

4.2.4 Conclusions

In summary, we report that the tip surface of rod-shaped $LiCoO_2$ nanoparticles, with high index surfaces such as (104), has higher ORR and OER activity as compared to the side with low index surfaces. In addition, the tip surface has larger specific charge transferred than the side for both Co 2+/3+ and 3+/4+ redox processes. The easier access to oxygen species and easier redox of under-coordinated Co atoms on high-index tip surfaces are used to explain the difference in catalytic performance between tips and sides. These findings showed that the surface catalytic reactions, such as OER and ORR, are closely related to surface terminations that determine the surface atomic and electronic structures of transition metals oxides. Therefore, the controlling and modification of surface terminations could be an effective way to design future catalysts.

Chapter 4, part 1, in full, is reprinted with permission from the following paper “Electronic spin transition in nanosize stoichiometric lithium cobalt oxide”, Journal of the American Chemical Society, 2012, 134(14), 6096-6099 by Danna Qian, Y. Hinuma, H.

Chen, L-S Du, K. Carroll, G. Ceder, C. P. Grey, Y. S. Meng, Copyright (2012) American Chemical Society. The second part, in part, is reprint from “The role of $LiCoO_2$ surface termination in oxygen reduction and evolution kinetics” being submitted by B. Han, Danna Qian (equally contributed), M. Risch, H. Chen, M. Chi, Y. S. Meng, Y. S-H.. The dissertation author was the primary investigator and author of the papers.

Figures:

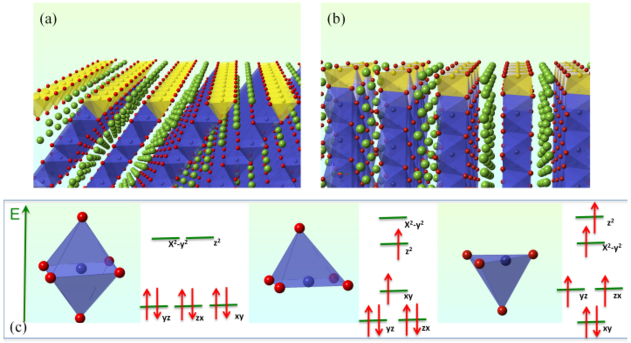

Figure 4.1: (a) {104} and (b) {110} surfaces of $LiCoO_2$ (c) Octahedrally, square pyramid and pseudo-tetrahedrally coordinated Co ions. (red- oxygen, green – lithium, blue – Co)

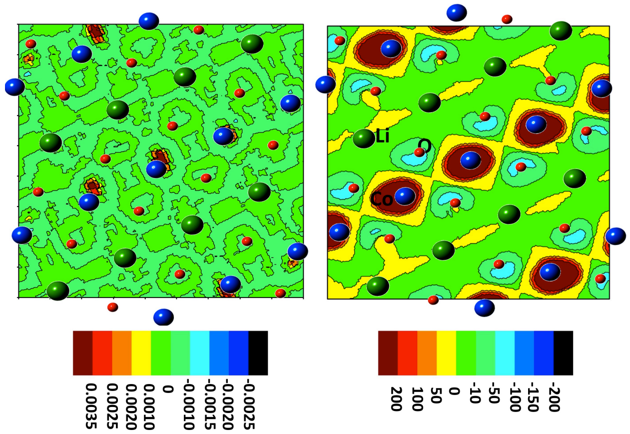

Figure 4.2: Spin density plot of the {104} plane of the bulk (a) and the surface (b). (Notice the scale differences in the spin density)

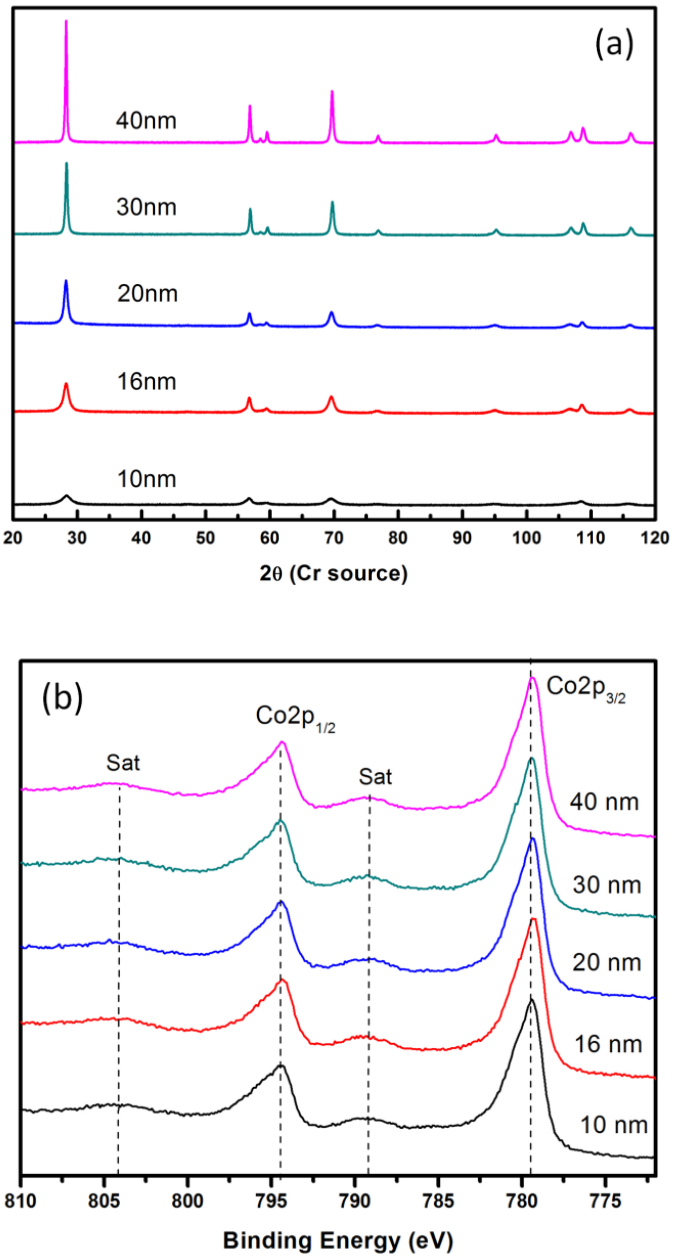

Figure 4.3: (a) XRD and (b) XPS spectra of nano-sized stoichiometric $LiCoO_2$.

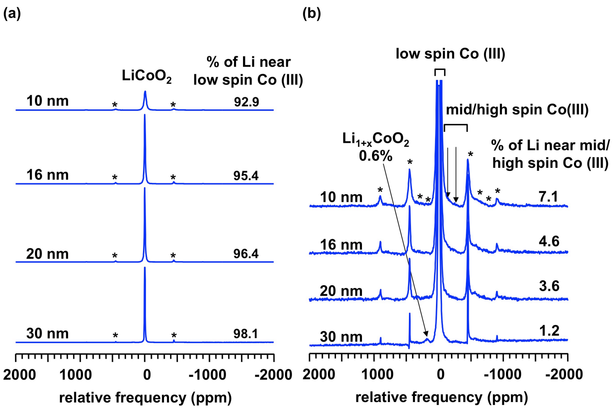

Figure 4.4: ^{7}Li MAS NMR spectra of $LiCoO_2$ with varying particle sizes. (a) Percentages of the Li near by low spin Co (III) in $LiCoO_2$ are listed in (a). Peak assignment and percentages of Li ions in environments nearby paramagnetic ions can be found in enlarged spectra. (b) Asterisks denote spinning sidebands.

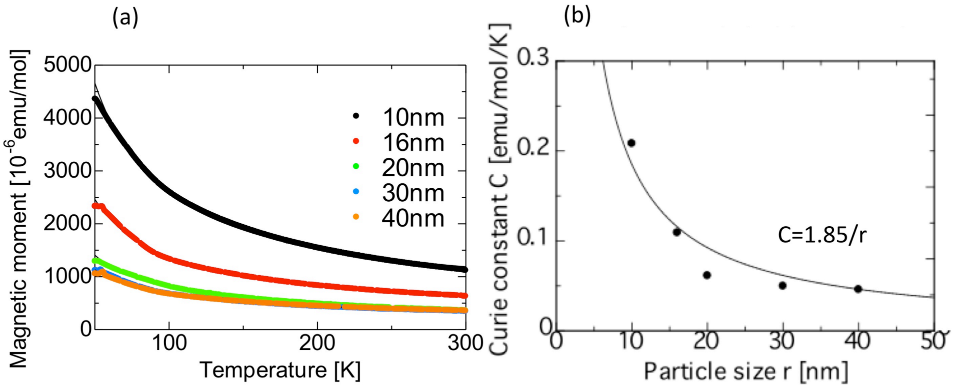

Figure 4.5: (a) Molar magnetic susceptibilities of particle size 10nm, 16nm, 20nm, 30nm and 40nm samples as a function of temperature. (b) The Curie constants of these samples determined from the $1/\chi$ vs T. (Both are measured with sample holder corrected)

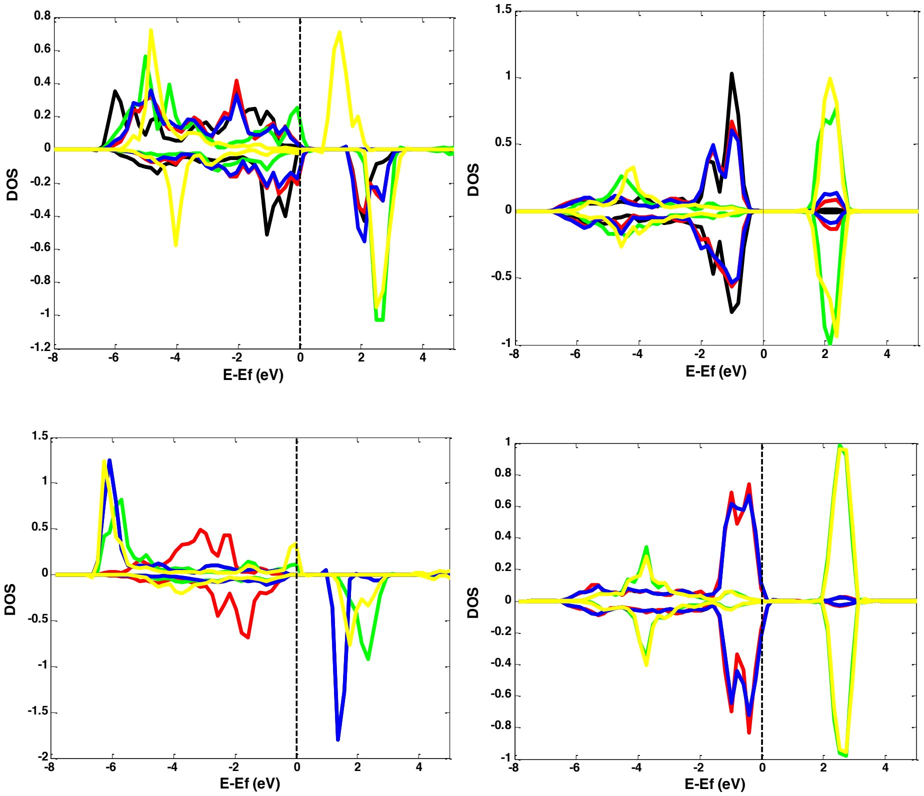

Figure 4.6: Projected density of states (DOS) of Co ions on the surface and bulk of $LiCoO_2$. Upper: {104} surface Co with IS (left) and bulk Co with LS (right); Bottom: {110} Surface Co with IS (left) and Bulk Co with LS (right)

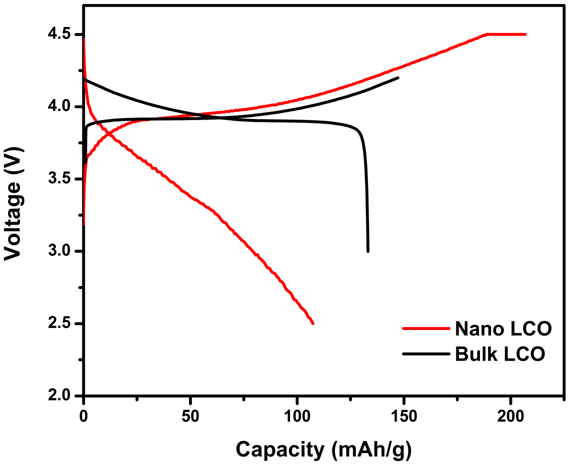

Figure 4.7: Electrochemical data for both bulk-$LiCoO_2$ (black) and 10nm-$LiCoO_2$ (red) in a lithium half-cell.

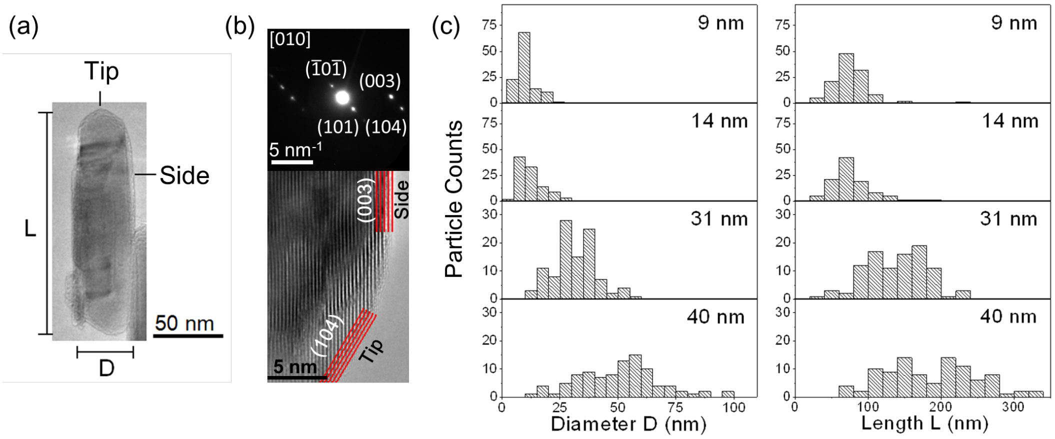

Figure 4.8: (a) Representative TEM image of a nanorod from the $LiCoO_2$ sample with an average rod diameter of 40 nm. (b) High-resolution TEM image of a representative nanorod $LiCoO_2$ with its associated selected-area electron diffraction pattern. (c) Histograms of the length and diameter distributions of different $LiCoO_2$ samples.

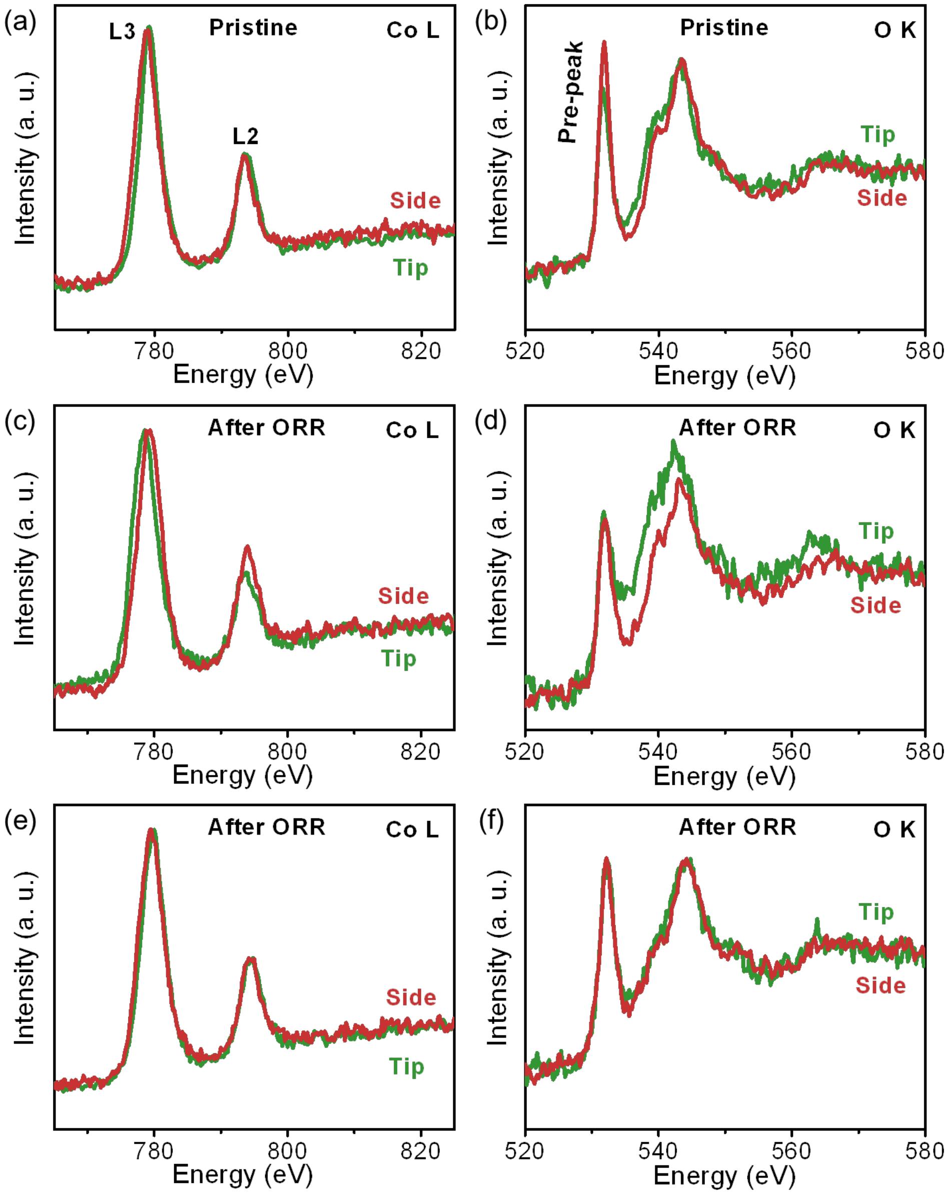

Figure 4.9: (a)(b) Representative EELS spectra of pristine 9-nm $LiCoO_2$: (a) Co L edge, (b) O K edge. (c)-(e) Two types of representative EELS spectra of 9-nm sample held at 0.7 V vs. RHE for ORR. Middle row is one set of (c) Co L edge and (d) O K edge (case 1); bottom row (e) and (f) is the other set of spectra (case 2). The analysis of O K pre-peak (at 532 eV) intensities can be found in Table 4.5.

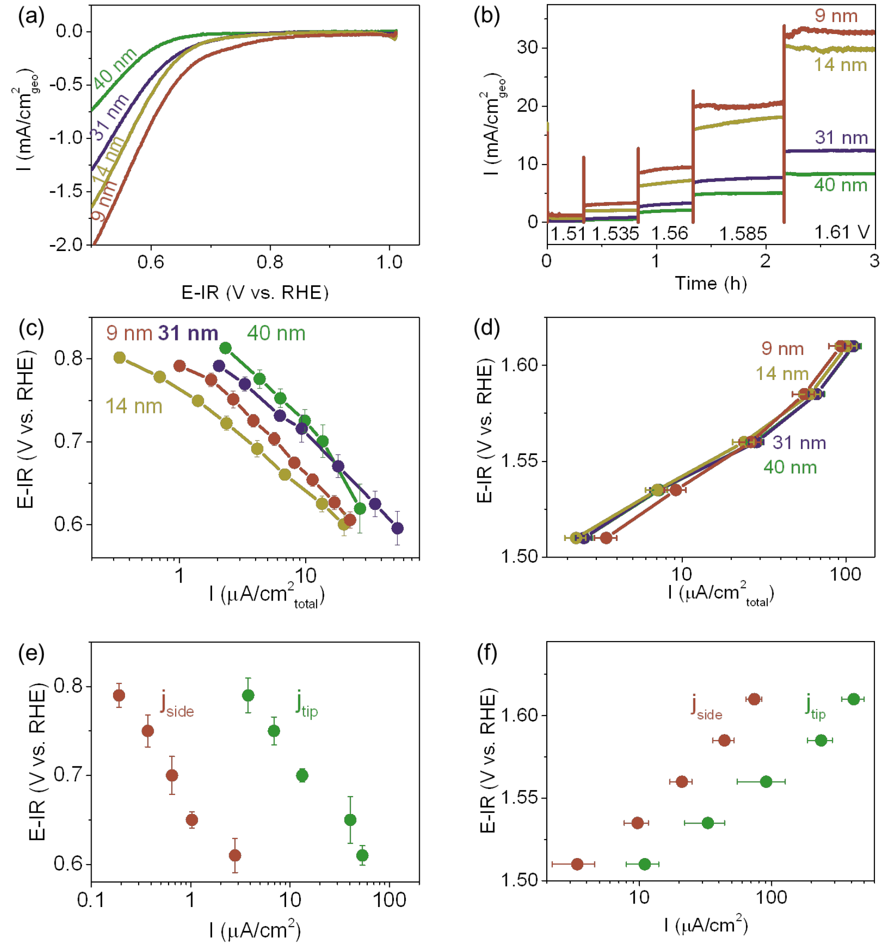

Figure 4.10: (a) Cyclic voltammetry of ORR current of different $LiCoO_2$ samples in O_2-saturated 0.1 M KOH at 10 mV/s. (b) Potentiostatic measurements of OER current of different $LiCoO_2$ samples in O_2-saturated 0.1 M KOH at different voltages. (c-f) Tafel plots of ORR and OER activities: (c) and (d) Tafel plots of ORR and OER activities of $LiCoO_2$ normalized by total surface area estimated from TEM particle size distribution,[94] respectively. The error bars represent the standard deviation of three different measurements for each sample. (d) and (f) Tafel plots of the specific ORR and OER activities of tip and side surfaces of $LiCoO_2$. The error bars were obtained from linear regression of j_{side} and j_{tip} .